REPORT

Area of Influence of mining activities in aquifers, salt caverns and cavern storage facilities

Client:	EBN
Archive no.:	EBN001_210723
Date:	23.07.2021

Q-con GmbH

Q-con GmbH
Marktstr. 39
76887 Bad Bergzabern
Germany

Email: info@q-con.de
Tel.: +49 (0) 6343 939699

Area of Influence of mining activities in aquifers, salt caverns and cavern storage facilities

Project:	Seismic Hazard Screening
Client:	EBN/ TNO-AGE
Archive no.:	EBN001_210723
Version:	210723
Date:	23.07.2021
Author(s):	Stefan Baisch, Christopher Koch
Checked by:	Robert Vörös
Approved by:	Robert Vörös

Contents

1 MASTER SUMMARY

1.1 Dutch

EBN werkt momenteel aan de ontwikkeling van een workflow voor seismiciteits risicoscreening (SHS) om het risico op geïnduceerde seismische activiteit van geothermische projecten te beoordelen. De SHS-workflow voorziet in een meer gedetailleerde geomechanische studie indien een geothermisch project gepland is in een regio met kritieke spanningen, terwijl het potentieel voor het induceren van seismiciteit door geothermische activiteiten laag wordt geacht in een niet-kritisch gespannen regio.

Als onderdeel van het grotere kader van de SHS-workflow, is de huidige studie (die overeenkomt met WP06 van de SHS-workflow) gericht op het schatten en in kaart brengen van het (mogelijk) kritisch gespannen invloedsgebied (AoI) van bestaande geotechnische installaties in Nederland, in het bijzonder gasvelden en -opslagen, zoutcavernes en caverne-opslag-installaties.

We hebben een eenvoudige benadering ontwikkeld om de AoI af te leiden op basis van volumeveranderingen in de ondergrond. Voor gas- en olievelden, waar de AoI wordt bepaald door depletie van de watervoerende laag, wordt een constante schaalfactor van 2,86 tussen reservoiroppervlak en AoI verkregen. Voor zoutcavernevelden, waar de AoI wordt gedomineerd door mechanische spanningsveranderingen, hangt de bijbehorende schalingsfactor af van het geproduceerde zoutvolume. Voor het grootste caverneveld omvat de AoI een bufferzone van 8,5 km, gemeten vanaf de veldgrenzen.

Wij hebben de AoI bepaald voor alle 197 geotechnische installaties (gas-/olievelden, zoutcavernes) onshore Nederland en KMZ-bestanden samengesteld die compatibel zijn met Google Earth. Elk KMZ-bestand bevat de laterale veldgrenzen en de AoI. Basisinformatie over het reservoir (formatiedoel, reservoirtype, seismiciteitsclassificatie, begin van de productie) wordt verstrekt als tags van de KMZ-bestanden.

Op basis van de door het KNMI gepubliceerde catalogus van geïnduceerde aardbevingen hebben wij geotechnische installaties geassocieerd met geïnduceerde seismiciteit, waarbij rekening is gehouden met onzekerheid in de plaatsbepaling. De resulterende classificatie van geïnduceerde seismiciteit maakt een onderscheid tussen "waarschijnlijk geassocieerd" (klasse A), "mogelijk geassocieerd" (klasse B) en "niet geassocieerd" (klasse C).

Op basis van de AoI's en de seismische classificatie stellen wij een puntensysteem voor om het potentieel aan geïnduceerde seismische activiteit voor een geothermisch project op een specifieke locatie in te schatten. De AoI's kunnen ook worden gebruikt voor het nemen van een binaire (ja/nee) beslissing of een geothermisch project zich al dan niet in een (mogelijk) kritisch gestresste regio bevindt.

De AoI's die in de huidige studie zijn afgeleid, zijn conservatief en overschatten waarschijnlijk

meestal het gebied waar kritieke spanningscondities kunnen heersen.

1.2 English

EBN is currently developing a seismic hazard screening (SHS) workflow to assess the induced seismicity risk of geothermal projects. The SHS workflow foresees a more detailed geomechanical study if a geothermal project is planned in a critically stressed region, while the potential for inducing seismicity by geothermal activities is considered low in a non-critically stressed region.

As part of the larger framework of the SHS workflow, the current study (corresponding to WP06 of the SHS workflow) aims at estimating and mapping the (possibly) critically stressed area of influence (AoI) of existing geotechnical installations in The Netherlands.

We have developed a simple approach for deriving the AoI based on subsurface volume changes. Assuming that the AoI is controlled by aquifer depletion, a constant scaling factor of 2.86 between reservoir area and AoI is obtained for gas- and oilfields. For salt-cavern fields, where the AoI is dominated by mechanical stress changes, the associated scaling factor depends on the produced salt volume. For the largest cavern field, the AoI includes a buffer zone of up to 8.5 km measured from the field boundaries.

We have determined the AoI for all 197 geotechnical installations (gas/oil fields, salt caverns) onshore The Netherlands and compiled KMZ files compatible with Google Earth. Each KMZ file includes the lateral field boundaries and the AoI. Basic reservoir information (geological period, reservoir type, seismicity classification, start of production) are added as tags to the KMZ files.

Based on the induced earthquake catalogue published by the KNMI, we have associated geotechnical installations with induced seismicity while accounting for location uncertainty. The resulting induced seismicity classification distinguishes between ‘likely associated’ (class A), ‘possibly associated’ (class B) and ‘not associated’ (class C).

Based on AoIs and seismicity classification, we propose a scoring scheme for ranking the induced seismicity potential of a geothermal project at a specific location. Alternatively, the AoIs can be used for making a binary (yes/no) decision whether a geothermal project is located in a (possibly) critically stressed region.

As by scope the AoIs derived in the current study are conservative and tend to overestimate the area over which critical stress conditions may prevail.

2 INTRODUCTION

2.1 Background

Exploiting geothermal energy through geothermal doublet systems is a relatively young technology in The Netherlands, which is currently promoted by the Dutch Ministry of Economic Affairs and Climate Policy. For safe implementation and technology upscaling, assessing and managing technology risks, including induced seismicity risks, is essential. Both, for geothermal project developers as well as for the regulator, it is important to get a first assessment of the project-specific induced seismicity risk by simple and practical means.

The current practise includes a so called Quick-Scan approach (Baisch et al., 2016) to assess the project-specific potential for inducing seismicity. The Quick-Scan score is a proxy, which is conceptually related to geomechanical processes that could cause seismicity.

Recently, the Quick-Scan approach has been reviewed and modifications were suggested to relate the screening approach more tightly to geomechanical processes (Mijnlieff & Jaarsma, 2021). Based on these suggestions, TNO-AGE and EBN are currently developing a new “seismic hazard screening (SHS)” workflow on the request of the Ministry of Economic Affairs. The SHS rests on the assumption that the natural stress state in the subsurface is not close to stress criticality over most of The Netherlands. Exceptions are the tectonically active Ruhr Valley Graben regions, as well as those regions, where anthropogenic activities may have altered subsurface stress conditions.

The SHS workflow foresees a more detailed geomechanical study if a geothermal project is planned in a (potentially) critically stressed region. On the other hand, the potential for inducing seismicity by geothermal activities is considered low in a non-critically stressed region.

2.2 Scope

EBN and TNO-AGE have commissioned several studies for outlining (potentially) critically stressed regions in The Netherlands. The current study, which corresponds to WP06 of the SHS workflow, aims at estimating and mapping the area of influence (AoI) of geotechnical installations (gas/oil fields, salt caverns) onshore The Netherlands.

As by request, the AoI should primarily capture the aspect of aquifer depletion due to mining activities. TNO-AGE and EBN seek a simple approach for estimating the field specific AoI. Previous (induced) seismicity should be related to individual geotechnical installations and a

scoring scheme shall be proposed, representing the induced seismicity potential in the vicinity of geotechnical installations.

Underestimating the AoI bears the risk that a causal relationship between earthquakes and geotechnical installations may not be recognized. Therefore, parameter uncertainties should be handled conservatively, implying that the AoI tends to be overestimated.

3 AREA OF INFLUENCE

3.1 Gas / Oil fields

For those fields, where gas or oil has been produced from the subsurface, it is assumed that the AoI is dominated by pressure depletion in hydraulically connected aquifers. Acknowledging that the spatial-temporal distribution of aquifer pressure depends on hydro-geological details and boundary conditions, we have chosen a first-order approximation based on the produced gas or fluid volume ΔV at reservoir conditions.

In this approach, the dynamic nature of the AoI is circumvented by conservatively approximating the conditions when the AoI reaches its maximum. The conceptual model (Figure 1) consists of the gas reservoir, connected to a vertically and horizontally confined aquifer. Confining the aquifer is a conservative assumption, as recharge from the far-field is ignored.

Assuming idealized and isothermal conditions, the general gas equation yields

Equation 1 $$\frac{\Delta V}{V} = -\frac{\Delta P}{P}\,.$$

Observations in The Netherlands indicate that induced seismicity has occurred in gas reservoirs at a relative depletion level of at least $\Delta P/P \geq 35\%$ (Van Wees et al., 2017). Assuming the same geomechanical processes for seismicity potentially induced in depleted aquifers, we define the AoI by its volume (compare Figure 1)

Equation 2 $$V_{AoI} = L_{AoI} \cdot W_{AoI} \cdot H_{AoI} \cdot \Phi'$$

such that

Equation 3 $$\frac{\Delta V}{V_{AoI}} = 35\%\,.$$

The apparent porosity Φ' is an averaged value corresponding to a homogeneous distribution of pore space over the entire block.

The theoretical production volume is given by

Equation 4 $$\Delta V = L \cdot W \cdot H \cdot \Phi'.$$

Assuming H_{AoI}=H and inserting Equation 2 and Equation 4 into Equation 3 yields

Equation 5 $$\frac{L \cdot W}{L_{AoI} \cdot W_{AoI}} = 35\%$$

implying that the lateral AoI is obtained by scaling the reservoir area by a factor of 2.86.

Based on shape files provided on nlog.nl (mei-2021-nlog-fields_utm.zip, downloaded 31.05.2021), 189 active or abandoned gas/oil fields onshore (+10 km) The Netherlands and two gas storage projects in salt caverns were identified. Some fields exhibit gas or oil reservoirs in several geological formations leading to a total number of 222 reservoirs. The area of each field was scaled by a factor of 2.86 while preserving the shape of the field boundaries. Resulting polygons were converted into KMZ files, which are accompanying this report (see section 3.3).

Several of the depleted gas reservoirs are now being used for underground gas storage (Bergermeer, Norg, Grijpskerk, Alkmaar). The (cyclic) gas storage volume is generally smaller than the gas volume initially produced, and gas storage may utilize only parts of the produced gas field. Therefore, the above AoI based on gas production already includes the smaller AoI resulting from gas storage.

For gas/oil reservoirs the aspect of aquifer depletion is considered most relevant in the reservoir formation itself. Due to the sealing nature of the cap rock, pressure perturbation, e.g. in the overburden, requires a permeable fault.

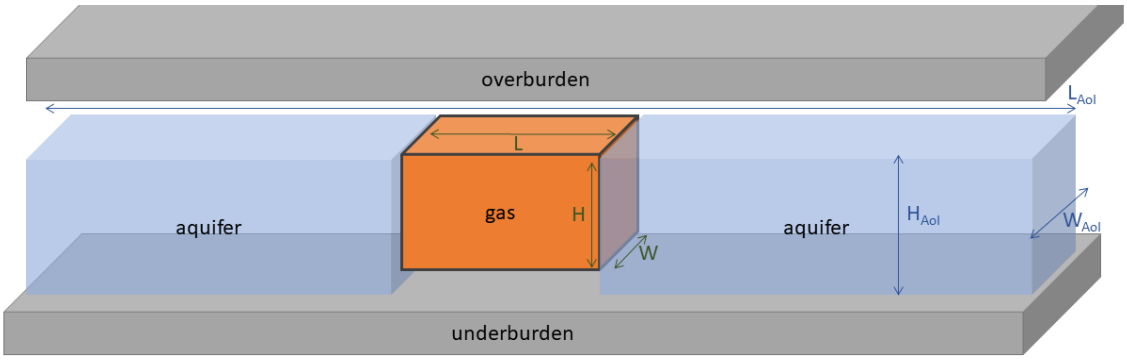

Figure 1: Conceptual sketch showing a gas filled reservoir, surrounded by an aquifer, and embedded into an impermeable over- and underburden.

3.2 Salt Caverns

It is assumed that salt caverns will collapse on a long timescale due to salt creep. As the caverns are generally filled with gas/fluid, cavern collapse is unlikely to cause aquifer depletion

and mechanical stresses are the dominating processes to potentially induce seismicity.

We use a geometrically simple representation of a cavern field (Figure 2) for numerically modelling Coulomb stress changes associated with complete cavern collapse.

We have determined the boundaries of the 6 salt cavern fields in The Netherlands visually in Google Earth using an overview of salt mining projects in the Netherlands (Staatstoezicht op de Mijnen, 2018) and the "Winningsplans" of salt mining projects (Paar, 2003; Well Engineering Partners B.V., 2012). Based on field boundaries and cumulative salt production volume ΔV (Table 1), we have approximated each of the salt cavern fields by 3 rectangular compaction sources, mimicking complete cavern collapse:

Equation 6 $$A_i \cdot d_i = \frac{\Delta V}{3} \qquad i=1,2,3$$

with source area A_i and dislocation d_i. The source area of the horizontal Okada source equals the area enclosed by the lateral field boundaries and the associated dislocation corresponds to the vertical compaction. Similarly, the source area of each of the two vertical Okada sources corresponds to the side length of the field times the reservoir height and the associated dislocation corresponds to the horizontal compaction.

Subsequently, we used Okada's semi-analytical solutions (Okada, 1992) for numerically simulating Coulomb stress changes ΔCS on optimally oriented normal faults. For the simulation we assumed parameters as listed in Table 2.

cavern field	ΔV [m^3]
Barradeel Zout	9,97E+06
Havenmond Zout	7,82E+04
Twente-Rijn Zout	1,23E+08
Veendam Zout	7,50E+06
Winschoten Zout (incl. Heiligerlee Stikstofbuffer)	3,69E+07
Zuidwending Zout	7,19E+07

Table 1: Cumulative salt production volume for salt cavern fields as of 2021. Data source: ARUP, 2018; Ruigrok et al., 2018; Staatstoezicht op de Mijnen, 2018; 'Winningsplans' published on nlog.nl. Data for Barradeel Zout and Havenmond Zout provided by TNO.

parameter	value
coefficient of friction	0.6
1st Lamé parameter	20 GPa
2nd Lamé parameter	20 GPa
Poisson ratio	0.25

Table 2: Parameters used for numerical simulation of Coulomb stress changes.

The model of a total cavern collapse may appear overly conservative as the timescale for total collapse can be large compared to the lifetime of a geothermal installation. We note, however, that stress perturbations caused by geothermal operations may remain in the subsurface long after geothermal reservoirs were abandoned. To ensure that the AoI estimate remains conservative even on a very long timescale, it was therefore decided to consider complete cavern collapse instead of partial collapse only.

Figure 3 shows simulated ΔCS for the largest cavern field Twente-Rijn Zout. Large Coulomb stress changes exceeding 10 MPa are obtained near the boundary of the cavern field at approx. 4.5 km distance from the centre (Figure 3, top). At larger distances, ΔCS is flattening out.

Defining the AoI requires an assumption on the level of stress changes resulting in critical conditions. The evidence-based approach used in the previous section is not directly applicable in the current context as pressure changes can only be converted into ΔCS within a geomechanical model. Observations from The Netherlands indicate that seismicity was induced by pressure changes in the order of 10 MPa (Thienen-Visser et al., 2012), but the associated seismicity is driven by poro-elastic stresses (e.g. Bourne et al., 2014), which could be significantly smaller than the driving pressure changes (e.g. Buijze et al., 2019).

Therefore, we have chosen a conservative assumption and defined the AoI at the ΔCS=1 MPa level.

For the Twente-Rijn Zout cavern field, this level is obtained at a critical distance of 10.9 km measured from the centre of the field (corresponding to a distance of up to approx. 8.5 km measured from the field boundaries).

From Figure 3 (bottom) we note that the AoI extends over up to 8 km also in the vertical direction. Therefore, we suggest applying the AoI of a salt cavern to the entire geothermal depth window.

Salt caverns are also used for gas storage at Winschoten and Zuidwending. The associated cavern volume used for gas storage has been included for computing the AoI of the cavern

fields. Therefore, the AoI of the cavern fields includes the (smaller) AoI resulting from gas storage.

cavern field	area scaling factor
Barradeel Zout	18
Havenmond Zout	26
Zuidwending Zout	440
Veendam Zout	15
Winschoten Zout (incl. Heiligerlee Stikstofbuffer)	182
Twente-Rijn Zout	18

Table 3: Area scaling factor for salt cavern fields. The area of the AoI is obtained by multiplying the area defined by the field polygon with the area scaling factor.

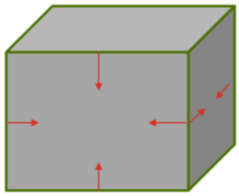

Figure 2: Schematic diagram showing compaction (red arrows) of a cube. Compaction occurs in three orthogonal directions.

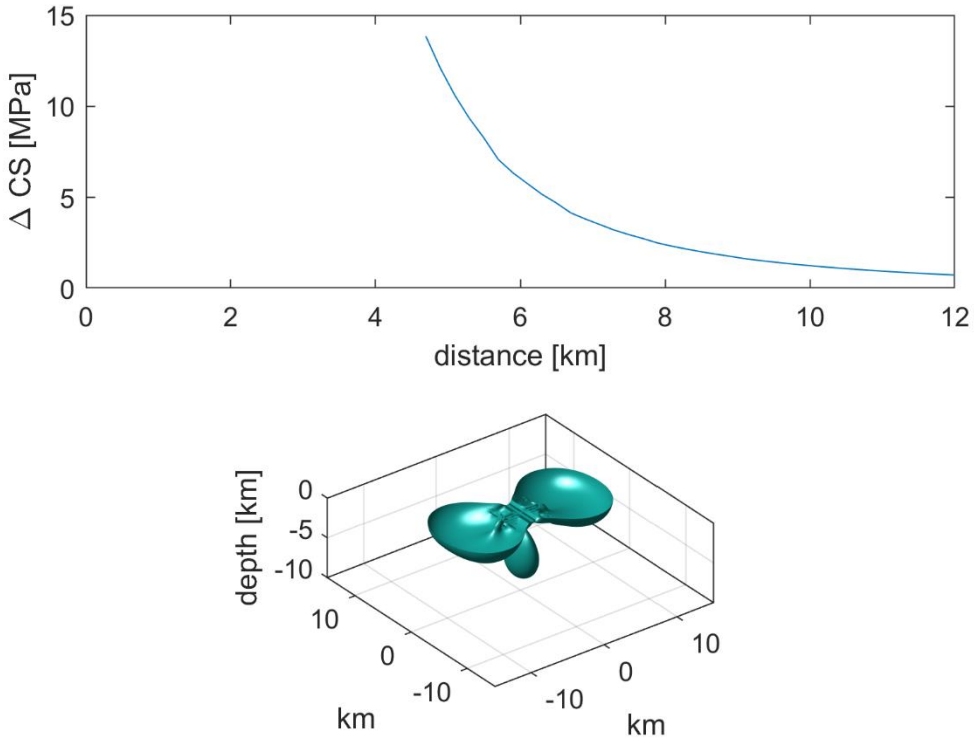

Figure 3: (top) Simulated maximum Coulomb stress changes ΔCS on optimally oriented faults (assuming normal faulting) as a function of distance for complete collapse of the Twente-Rijn Zout cavern field. Distance measured with respect to the centre of the cavern field and maximum stress changes refer to the maximum in an arbitrary direction. (bottom) Isosurface shown at ΔCS=1 MPa to visualize the spatial distribution of Coulomb stress changes. Origin of the coordinate system corresponds to the centre of the cavern field.

3.3 KMZ Files

KMZ files compatible with Google Earth were compiled individually for the AoI of each geotechnical installation. Each KMZ file includes the lateral field boundaries and the AoI. Basic reservoir information (geological period, reservoir type, seismicity classification, start of production) are added as tags to the KMZ files.

4 INDUCED SEISMICITY CLASSIFICATION

The occurrence of induced seismicity is a multi-parameter phenomenon requiring a specific constellation of different subsurface parameter combinations (e.g., Buijze et al., 2019; Vörös & Baisch, 2018). Therefore, the AoI can only refer to a region in which a certain level of stress

perturbations can cause seismicity, without predicting that seismicity will actually occur at this level of stress perturbations.

This is quite different if a reservoir has already produced seismicity, providing direct evidence for stress criticality at this location. Obviously, seismogenic reservoirs are of particular importance in the context of seismic hazard screening, which is also accounted for in the proposed scoring scheme in chapter 5.

Based on the induced earthquake catalogue published by KNMI (https://www.knmi.nl/kennis-en-datacentrum/dataset/aardbevingscatalogus, downloaded 07.06.2021), we have associated geotechnical installations with induced seismicity.

Our approach closely follows a previous study (Vörös & Baisch, 2018), where we used a global epicentre location uncertainty of 2.5 km for testing whether or not induced earthquakes could be moved into a gas field within location uncertainty. The global estimate of location uncertainty is motivated by numerical simulations of the location uncertainty of the KNMI network geometry at different times (Baisch et al., 2017).

Different to our previous approach, we have based the analysis on AoI rather than on field boundaries and used the classification system summarized in Table 4. Figure 4 to Figure 6 show maps of the resulting field classification. Acausal correlations, i.e. if an earthquake has occurred prior to field operations, were ignored.

It is important to notice that the classification of a field may change over time. For example, if a new earthquake has occurred or if the analysis of historic seismicity yields different earthquake locations and/or location uncertainties. In this case, the KMZ data base (section 3.3) needs to be updated. The updating process is described in chapter 6.

Category	Description
A – likely associated with seismicity	Earthquakes are located inside AoI of field
B – possibly associated with seismicity	Earthquakes located at 2.5 km distance to AoI of field
C – not associated with seismicity	No earthquakes located within 2.5 km distance to AoI of field

Table 4: Induced seismicity classification scheme.

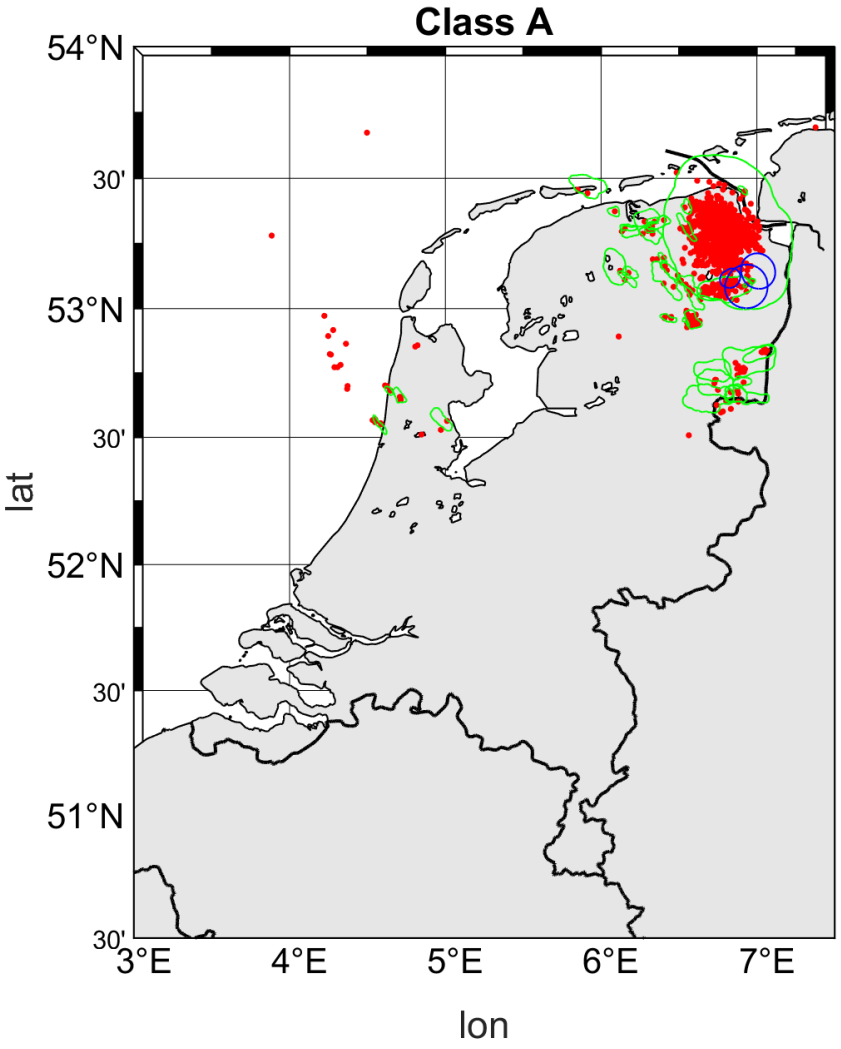

Figure 4: Induced seismicity (red dots) and AoI of Class A oil/gas fields (green contours) and salt caverns (blue contours).

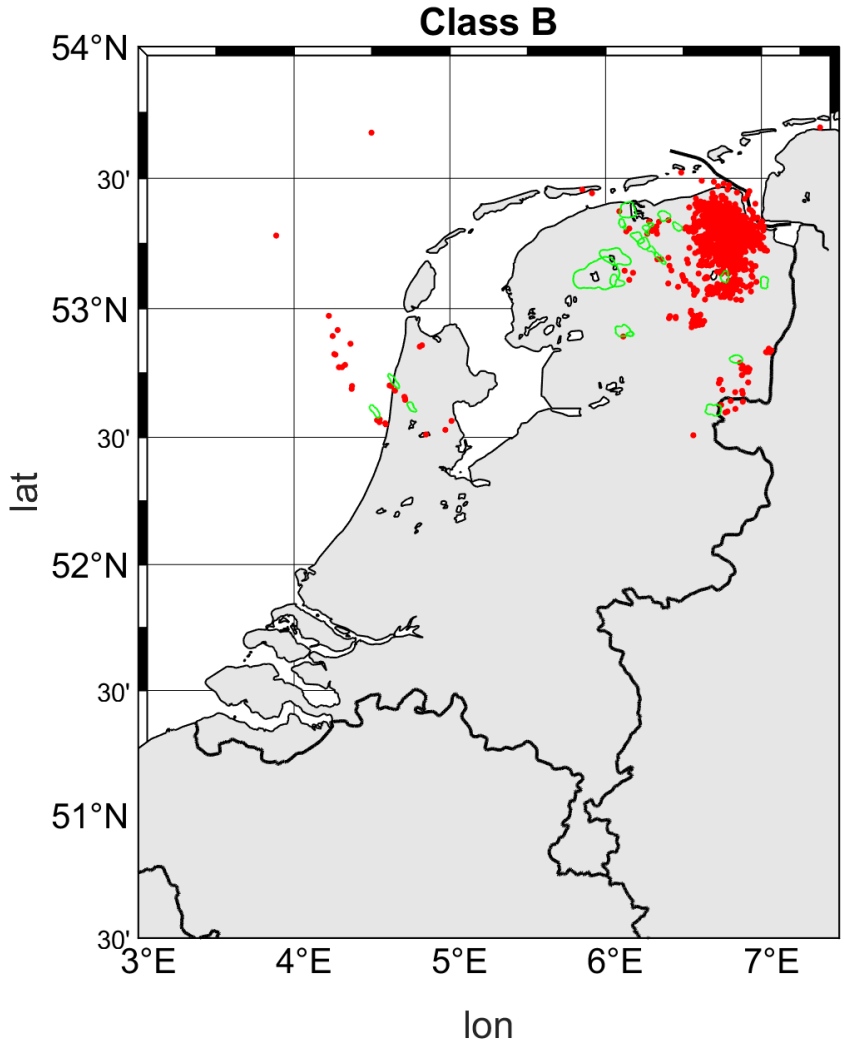

Figure 5: Induced seismicity (red dots) and AoI of Class B oil/gas fields (green contours) and salt caverns (blue contours).

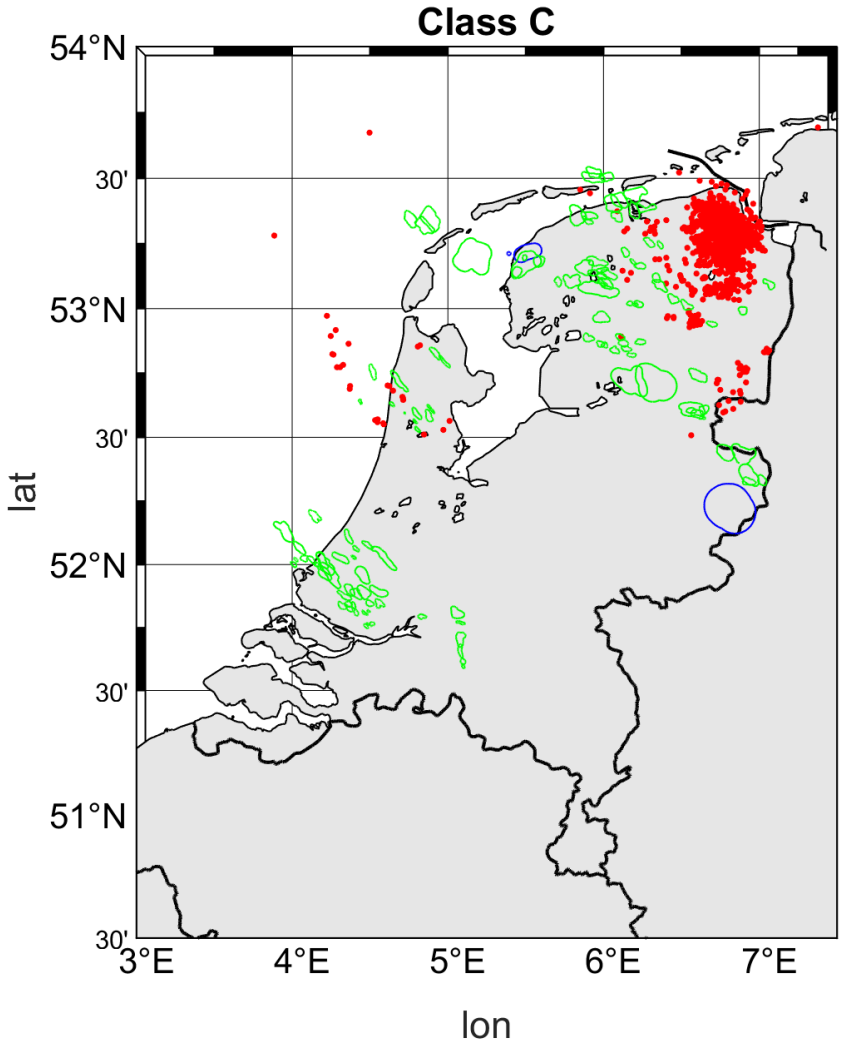

Figure 6: Induced seismicity (red dots) and AoI of Class C oil/gas fields (green contours) and salt caverns (blue contours).

5 SCORING SCHEME

The AoI of salt caverns has a significant component also in vertical direction and we suggest applying the same AoI to all depth levels of geothermal exploration (section 3.2).

This is different for gas and oil fields, where aquifer depletion is mostly restricted to the reservoir formation (section 3.1). Following a conservative approach, we suggest considering the possibility of aquifer depletion also in the over- and underburden. To ensure sufficient vertical safety distance also in case of thin layering, reservoirs may be grouped according to their geological age (Table 5) and over- / underburden may be defined by geological age. Alternatively, these definitions could be made specifically for a planned geothermal project by considering the local stratigraphy.

At this stage, TNO-AGE and EBN have not decided whether the seismic hazard screening will be based on a binary (yes/no) evaluation of key factors or on a scoring scheme. The following suggestions support both options:

(1) The AoI (including the over-/underburden) already provides the basis for a binary (conservative) evaluation of stress criticality.
(2) If information of previous seismicity should be included, we propose the scoring schemes summarized in Table 6 and Table 7. Higher scores denote larger potential for inducing seismicity.

Carboniferous
Rotliegend
Zechstein
Triassic
Jurassic
Cretaceous
Tertiary

Table 5: Geological age for defining over-/underburden.

Class	Distance to AoI	Formation	Score
A	Inside	Same	10
B	Inside	Same	8
C	Inside	Same	5
A	Inside	overburden/underburden	7
B	Inside	overburden/underburden	5
C	Inside	overburden/underburden	3
A,B,C	Outside	same/over-/underburden	0

Table 6: Scoring scheme proposed for oil / gas fields including gas storage. The parameter 'class' refers to the induced seismicity classification summarized in Table 4.

Class	Distance to AoI	Formation	Score
A	Inside	same/over-/underburden	10
B	Inside	same/over-/underburden	8
C	Inside	same/over-/underburden	5
A,B,C	Outside	same/over-/underburden	0

Table 7: Scoring scheme proposed for salt cavern fields including gas storage.

6 GUIDELINES FOR FUTURE UPDATES

The AoIs derived in this study reflect the current state of knowledge regarding subsurface activities and related seismicity. Changes in exploration as well as new interpretations and future observations may require an update of the AoIs and their classification.

6.1 Seismicity Classification

Most relevant in this context is the change of the seismicity classification following future seismicity and/or re-locating historic seismicity. For example, 12 class A fields ("*likely associated"*) and 10 class B fields ("*possibly associated"*) are associated with a single earthquake only (Table 8 and Table 9). If earthquake specific epicentre location errors were determined for the associated earthquakes (Table 10), then the resulting confidence ellipsoids could be visually compared to the field AoIs in Google Earth. Fields where the AoI is intersected by a confidence ellipsoid fall into class B, other fields with no intersections fall into class C (*"not associated"*). Any change of the seismicity classification could be directly applied to the field tag in the KMZ file.

Bergen	Emmen-Nieuw Amsterdam	Emshoern	Houwerzijl	Kollum-Noord	Marum
Metslawier	Middelie	Pasop	Ureterp	Warffum	Zuidwending-Oost

Table 8: List of Class A fields associated with a single earthquake only.

Anjum	Grootegast	Leeuwarden-Nijega	Noordwolde	Opeinde-Zuid
Oude Pekela	Pieterzijl Oost	Sebaldeburen	Tietjerksteradeel	Weststellingwerf

Table 9: List of Class B fields associated with a single earthquake only.

09-Sep-1994 15:56:54	02-Mar-1997 15:25:32	22-Apr-1999 22:58:02	10-Oct-2001 06:41:09
14-Feb-2003 06:54:24	28-May-2005 19:57:57	23-Apr-2006 15:02:07	26-Nov-2009 12:54:14
07-Dec-2009 00:24:59	27-Jan-2012 06:18:32	10-Jul-2012 18:09:09	01-Mar-2015 16:32:47
30-Oct-2016 20:58:19	04-Jun-2018 23:01:02	04-Aug-2019 10:26:29	23-Jan-2020 03:48:05
22-Feb-2020 18:12:55			

Table 10: List of earthquakes associated with the fields listed in Table 8 and Table 9.

6.2 AoI Gas/Oil Fields

The AoI of a gas or oil field needs to be (re-)computed if

i. a new field starts producing,
ii. field boundaries are re-interpreted (i.e. the field polygon changes),
iii. the assumed level of stress criticality (Equation 3) changes.

In all cases, the same workflow can be applied as outlined below. We have implemented the workflow in MATLAB, but other programming languages are equally well suited.

(1) Start with the lateral field polygon in rectangular coordinates (e.g. UTM).
(2) Compute the polygon area.
(3) Derive the area scaling factor using Equation 3.
(4) Scale the polygon by a factor *k* while preserving its shape. We have used an algorithm that is rounding out boundary joints. Adjust the scaling factor *k* such that the resulting polygon area is scaled by the factor determined in step (3). We have used a non-linear optimization (Nelder-Mead) approach to exactly match the area scaling factor.
(5) Export the scaled polygon as KMZ or shape file.

6.3 AoI Salt Caverns

The AoI of a salt cavern needs to be (re-)computed if

i. a new field starts producing,

ii. field boundaries are re-interpreted (i.e. new cavern(s) start(s) producing),

iii. the production volume of an existing field changes,

iv. the assumed level of stress criticality (currently 1 MPa) changes.

In all cases, the same workflow can be applied as outlined below. We have implemented the workflow in MATLAB, but other programming languages are equally well suited.

(1) Start with the lateral field polygon in rectangular coordinates (e.g. UTM).
(2) Compute the polygon area A_{pol}.
(3) Define 3 equivalent Okada sources. The rectangular sources are orthogonal to each other's. The base area of the horizontal source corresponds to the polygon area A_{pol}. The base area of the two vertical sources corresponds to $\sqrt{A_{pol}} \cdot H$.
(4) Use Okada's semi-analytical solutions for simulating ΔCS as described in section 3.2 and determine the critical distance r_{crit} over which ΔCS exceeds the assumed level of stress criticality.
(5) Calculate the scaling factor $f = \frac{\pi \cdot r_{crit}^2}{A_{pol}}$.
(6) Scale the polygon by a factor f while preserving its shape. We have used an algorithm that is rounding out boundary joints. Adjust the scaling factor f such that the resulting polygon area is scaled by the factor determined in the previous step. We have used a non-linear optimization (Nelder-Mead) approach to exactly match the polygon area.
(7) Export the scaled polygon as KMZ or shape file.

7 REFERENCES

ARUP. (2018). *Salt Mine Seismicity - Document Review and Initial Recommendations – Rev A* (Technical Note) (p. 12). London, UK: ARUP.

Baisch, S., Koch, C., Stang, H., Pittens, B., Drijver, B., & Buik, N. (2016). *Defining the Framework for Seismic Hazard Assessment in Geothermal Projects V0.1 - Technical Report* (No. 161005) (p. 65).

Baisch, S., Vörös, R., Koch, C., Stang, H., & Rothert, E. (2017). *Recommendations for a Traffic Light System limiting the strength of seismicity induced in small gas fields in The Netherlands* (No. 170601_SODM001) (p. 91). Bad Bergzabern: Q-con GmbH.

Bourne, S. J., Oates, S. J., van Elk, J., & Doornhof, D. (2014). A seismological model for earthquakes induced by fluid extraction from a subsurface reservoir. *Journal of Geophysical Research: Solid Earth*, *119*(12), 8991–9015. https://doi.org/10.1002/2014JB011663

Buijze, L., Bogert, P. A. J., Wassing, B. B. T., & Orlic, B. (2019). Nucleation and Arrest of Dynamic Rupture Induced by Reservoir Depletion. *Journal of Geophysical Research: Solid Earth*, *124*(4), 3620–3645. https://doi.org/10.1029/2018JB016941

Buijze, L., van Bijsterveldt, L., Cremer, H., Paap, B., Veldkamp, H., Wassing, B. B. T., et al. (2019). Review of induced seismicity in geothermal systems worldwide and implications for geothermal systems in the Netherlands. *Netherlands Journal of Geosciences*, *98*, e13. https://doi.org/10.1017/njg.2019.6

Mijnlieff, H., & Jaarsma, B. (2021). *Voorstel voor Aanpassing van de Methodiek voor Screening van Seismiciteitsdreiging bij Geothermie - Finale Versie Februari 2021 -* (Final version) (p. 39). TNO-AGE/ EBN.

Okada, Y. (1992). Internal deformation due to shear and tensile faults in a half-space. *Bulletin*

of the Seismological Society of America, *82*(2), 1018–1040.

Paar, W. A. (2003). *Winningsplan voor de winningsvergunnning Adolf van Nassau (boorterrein Winschoten/Heiligerlee)* (No. 0310301 HL). Hengelo.

Ruigrok, E., Spetzler, J., Dost, B., & Evers, L. (2018). *Winschoten events, 19-11-2017* (Technical Report No. TR-318) (p. 27). De Bilt: KNMI.

Staatstoezicht op de Mijnen. (2018). *Staat van de sector zout*. Den Haag: Staatstoezicht op de Mijnen.

Van Wees, J.-D., Fokker, P. A., Van Thienen-Visser, K., Wassing, B. B. T., Osinga, S., Orlic, B., et al. (2017). Geomechanical models for induced seismicity in the Netherlands: inferences from simplified analytical, finite element and rupture model approaches. *Netherlands Journal of Geosciences*, *96*(5), s183–s202. https://doi.org/10.1017/njg.2017.38

Vörös, R., & Baisch, S. (2018). *Geomechanical Study – Small Gas Fields in the Netherlands* (No. SODM002) (p. 57). Bad Bergzabern: Q-con GmbH.

Well Engineering Partners B.V. (2012). *Winningsplan voor winningsvergunning "Havenmond" Actualisatie v.4.5* (No. revision v. 4.5). Well Engineering Partners B.V.